IEEE Open Journal of
Power Electronics

Received 10 October 2021; revised 8 December 2021 and 15 December 2021; accepted 16 December 2021. Date of publication 21 December 2021; date of current version 6 January 2022. The review of this article was arranged by Associate Editor Liangzong He.

Digital Object Identifier 10.1109/OJPEL.2021.3137016

Fully-Integrated Solid Shunt Planar Transformer for LLC Resonant Converters

SAJAD A. ANSARI, JONATHAN N. DAVIDSON, AND MARTIN P. FOSTER

Department of Electronic and Electrical Engineering, University of Sheffield, S1 3JD Sheffield, U.K.

CORRESPONDING AUTHOR: SAJAD A. ANSARI (e-mail: sarabansari1@sheffield.ac.uk)

This work was supported by the Engineering and Physical Sciences Research Council (EPSRC) under Grant EP/S031421/1.

ABSTRACT A new topology for achieving high leakage inductance in inserted-shunt integrated magnetic planar transformers is proposed. In the proposed topology, two one-segment shunts are placed across the planar E-core air gap and between the primary and secondary windings. The proposed topology benefits using solid inexpensive ferrite shunts, making manufacturing easier. A detailed mathematical model is derived from which a design methodology is developed, providing accurate estimation for the leakage and magnetising inductances. The theoretical analysis has been verified using finite-element analysis and experimental implementation. AC resistance analysis and efficiency comparison are also presented for the proposed topology and a recent topology with inserted-segmental-shunt, which shows the proposed topology provides higher efficiency because of lower AC resistance. In addition, an isolated LLC resonant converter is designed and built to investigate the performance of the proposed topology in practice. The three magnetic components needed for the designed LLC resonant converter is integrated in a single planar transformer using the proposed topology and the converter operates properly.

INDEX TERMS High-permeability materials, integrated magnetic transformer, LLC resonant converter, segmental shunt, solid shunt.

I. INTRODUCTION

Hard-switched pulse-width-modulated (PWM) converters such as the buck and boost converters cannot be operated at high frequency under continuous conduction mode (CCM) since they suffer from high switching losses under high-frequency operation. Hence, their switching frequency needs to be limited to achieve high efficiency, leading to lower power density [1]–[5]. Research has attempted to provide a soft-switching capability for hard-switched converters; however, solutions are mainly based on adding various auxiliary circuits to the topology of the hard-switched converters, which increases their complexity and cost [6]–[8].

Resonant converters are displacing traditional hard-switched converters because they benefit from soft-switching capability inherently and can provide high efficiency at high frequency operation [9]. Amongst resonant converters, the interest in the LLC topology, shown in Fig. 1, has increased because of its excellent soft-switching performance, low voltage stress of switching devices and integration of magnetic components [10]–[12]. As shown in Fig. 1, an isolated LLC converter needs multiple magnetic components consisting of a series (also known as "resonant") inductor, a parallel inductor and a transformer.

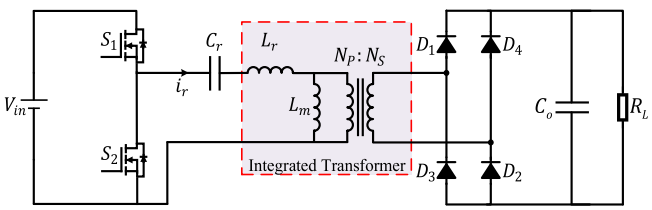

FIGURE 1. Topology of the half-bridge LLC resonant converter.

To increase the power density and efficiency, and decrease the cost of an LLC converter, its magnetic components can be integrated into a single magnetic transformer. An auxiliary winding can be added to the transformer for integration of transformer and inductor cores [13]–[16]. In this structure, the winding of the series inductor is coiled around one leg

of transformer core and primary and secondary windings are on other legs.

Another way to integrate the required series inductance into the transformer is to produce a design-specific core geometry or add an auxiliary core to a standard-geometry transformer and merge either the primary winding or secondary winding with the winding of series inductor [14], [17]–[20]. Even though the required series inductance can be integrated into the transformer using this method, this approach requires a new, bespoke transformer core for each design.

In [21], the primary and secondary windings are looped around the outer-left and outer-right legs of the transformer and an air gap is inserted into the centre leg of the E-core to achieve a controllable leakage inductance. Although a simple multi-layer PCB with minimal complexity can be used as the windings, the transformer has a large footprint since the windings extend outside the transformer core. In addition, the AC resistance is high in this design, and leakage and magnetising inductances are not decoupled and cannot be designed separately.

A lower AC resistance and controllable leakage inductance can be achieved with an interleaved or a semi-interleaved windings structure and core shape of the transformer [22], [23]. However, the winding structure is complicated in these approaches and the leakage and magnetising inductances are not decoupled and affect each other's value which makes the design process more complicated. In addition, the windings are looped around the outer legs, leading to lower power density.

The leakage inductance of a typical wound-core transformer can be selected by design and used as the series inductance of the LLC topology [24]–[26]. However, flexibility of design is limited in this method since the leakage inductance is mainly affected by the geometry of the core and windings and thus cannot be regulated for different values easily.

Some magnetic sheets can be also added between layers of windings to integrate the magnetic components by enhancing the leakage inductance (as a result of increasing energy stored in the window area) [27]. However, this approach suffers from lower efficiency due to the high eddy-current losses in the windings and low flexibility in design. In addition, a high leakage inductance cannot be designed in this structure.

An LLC resonant converter with high series inductance can provide high voltage gain within a narrow operating frequency range, which is needed for applications with wide input voltage range. Therefore, the increase of leakage inductance, which is the series (resonant) inductance in an LLC topology, is an important consideration in integrated transformers [27], [28]. Inserting a low-permeability magnetic shunt in the centre of a planar transformer while its primary and secondary windings are separated (by being located above and below the magnetic shunt) can provide a high leakage inductance and provides greater and more precise control of its value [29]–[31]. This topology also benefits from the advantages of planar transformers, viz high power density, improved cooling capability, modularity and manufacturing simplicity. In this topology, all three magnetic components of an isolated LLC converter can be integrated in a single planar transformer. Even though this structure enhances the leakage inductance and allows for its value to be estimated precisely, the inserted shunt must have a specific and unusually low permeability, leading the design and manufacturing to difficulty and higher cost.

A new topology is suggested in [32]–[34] to overcome this problem. These structures, are formed by interleaving highly permeable ferrite with thin plastic spacers to form segmental magnetic shunts. Fig. 2(a) shows this topology when a two-segment shunt is used and this topology with five-segment shunt can also be found in [32], [33]. In this structure, a shunt with the same bulk permeability as the conventional design (which uses a low-permeability shunt) is approximated by regulating the length of the air gaps between segments across the high-permeability shunt. Although this structure eliminates the need for shunts with specific permeabilities and dimensions, the inserted shunt has multiple segments and has to be placed in between two E-cores which makes the implementation difficult.

To address this issue, a new structure shown in Fig. 2(b) is proposed in this paper. In the proposed topology, two solid shunts are placed on the front and back (x-y plane) of a planar transformer while primary and secondary windings are separated by being located above and below the shunts such that some of the primary winding generated flux is shunted away from the secondary winding in order to realise the leakage inductance. The bulk permeability of the shunts is regulated by changing their distance from the core (ℓ_s). Therefore, not only does the proposed structure benefit from using high-permeability materials for the shunts but its inserted shunts also do not need to be segmental and can be located easier. The proposed structure is analysed and modelled and a design guideline is also provided. The theoretical analysis is verified by comparison with finite-element analysis (FEA) simulation and experimental measurements. The AC resistance analysis and efficiency comparison for the proposed structure and a recent structure with inserted-segmental-shunt presented in [32], [33] are provided. In addition, in order to examine the performance of the proposed structure in practice, an isolated LLC resonant converter using the proposed integrated transformer is implemented and investigated. The prototype proves that the proposed structure can integrate all three magnetic components of an LLC converter in a single planar transformer.

The paper is organised as follows: the modelling of the proposed inserted-solid-shunt integrated transformer is presented in Section II. In Section III, a simulation study is provided to show the accuracy of the theoretical analysis. Experimental results are provided in Section IV to validate theoretical and finite-element analyses and integration capability of the proposed structure. The conclusion of the work is finally presented in Section V.

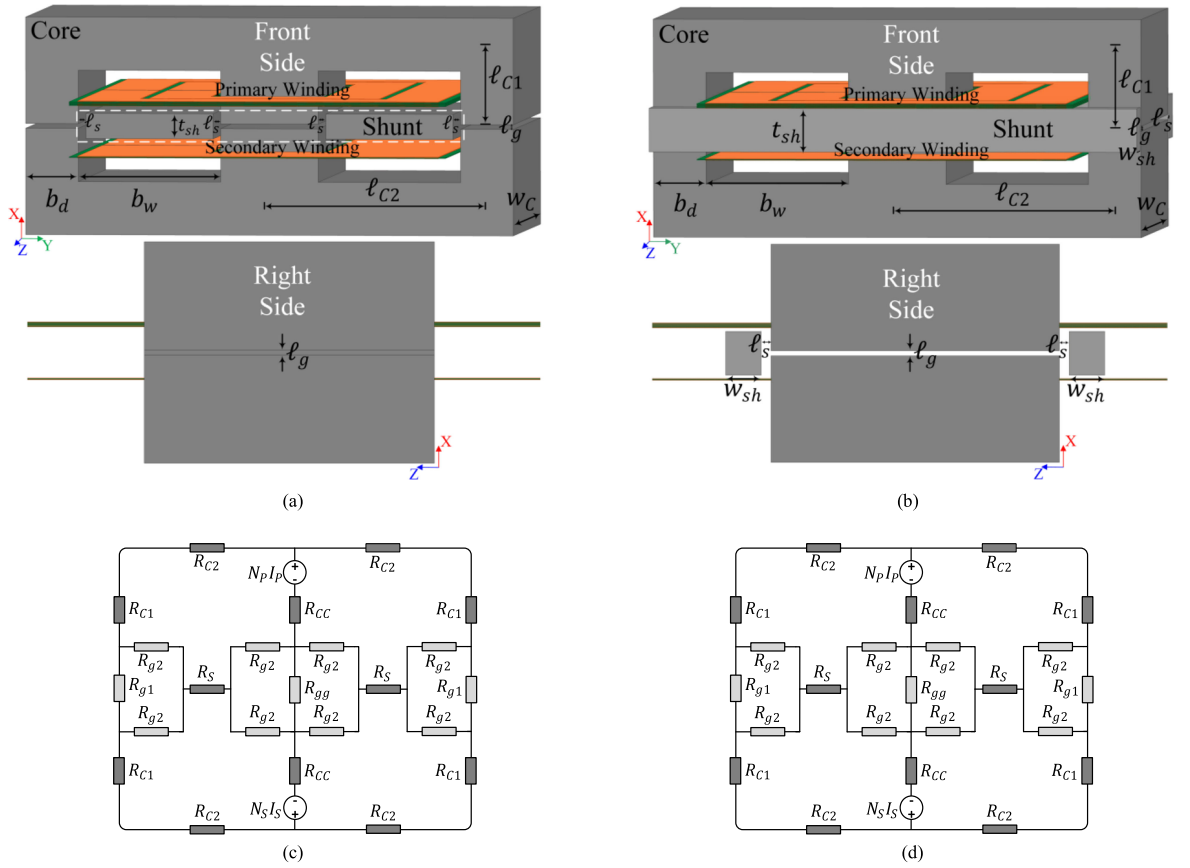

FIGURE 2. **The inserted-shunt integrated planar transformer. (a) Schematic of inserted-segmental-shunt topology. (b) Schematic of proposed topology. (c) Reluctance model of inserted-segmental-shunt topology. (d) Reluctance model of proposed topology.**

II. PROPOSED INTEGRATED MAGNETIC TRANSFORMERS

The topology of an inserted-segmental-shunt integrated planar transformer presented in [32], [33] and its reluctance model are shown in Figs. 2(a) and (c), respectively. As shown, a segmental shunt is inserted between the E-cores in line with air gap, and the primary and secondary windings are separated by being placed above and below the segmental shunt. In this topology, the leakage inductance can be regulated by changing the thickness of the shunt, t_{sh}, and the shunt air gap length, ℓ_s, and the magnetising inductance can be regulated by air gap length, ℓ_g, separation between the E-cores. This topology guarantees a high leakage inductance and accurate estimation of its value. However, the difficulty with this topology is locating the segmental shunt in between the E cores and requiring a segmental shunt (minimum two segments), which results in manufacturing difficulty. To address this issue, a new topology for the integrated transformer is proposed, which benefits from overlaying the solid shunt across the E-core air gap and thereby simplifying manufacture.

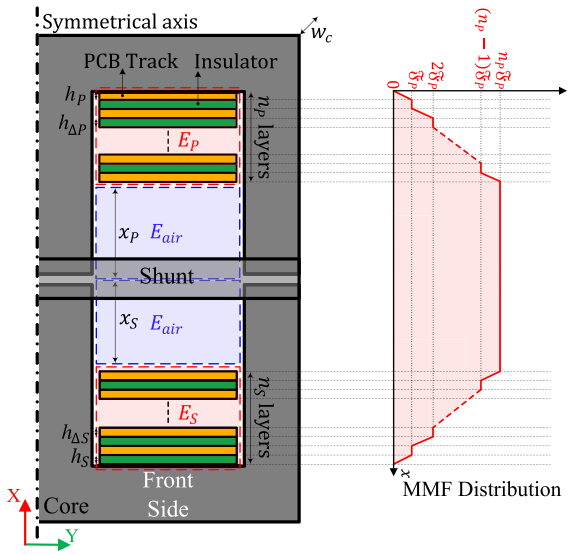

FIGURE 3. **MMF distribution for the proposed structure.**

The schematic of the proposed topology and its reluctance model are shown in Figs. 2(b) and (d), respectively. In the proposed topology, two solid shunts are placed on the front and back of a planar transformer and between the primary and secondary windings which are separated by being located at opposite sides away from the magnetic shunts. The air gap ℓ_g is inserted in between the E-cores to regulate magnetising inductance and the air gap ℓ_s is added in between the shunts and E-cores to regulate the leakage inductance. As shown in Fig. 2, the proposed topology provides the same reluctance

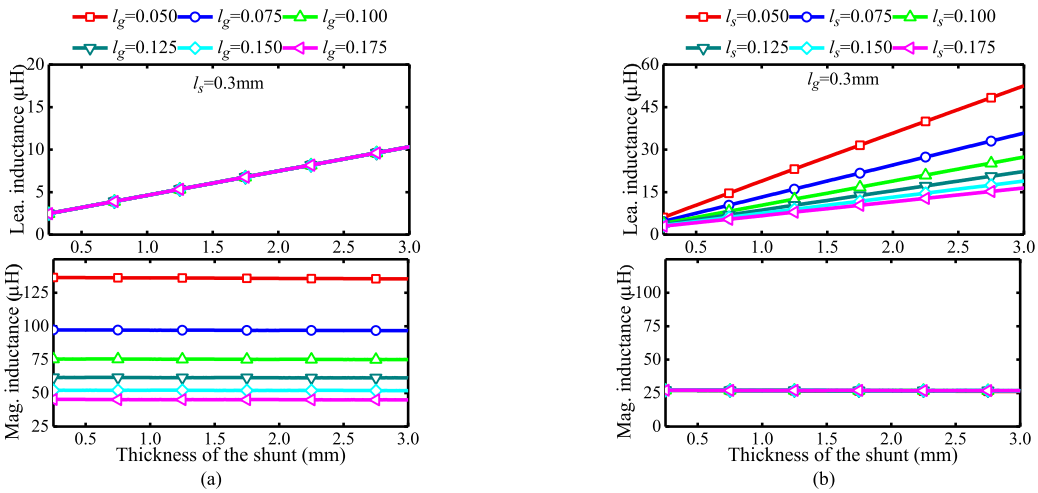

FIGURE 4. The calculated leakage and magnetising inductance versus thickness of the shunt. (a) For different E-core air gaps (ℓ_g). (b) For different distances from shunts to cores (ℓ_s). Core: E32/6/20/R-3F4, ℓ_g and ℓ_s in mm, w_{sh}=2.5mm, N_P=10, N_S=2, n_P=5, n_S=2, k_P=2, k_S=1, x_P= x_S=1.5mm.

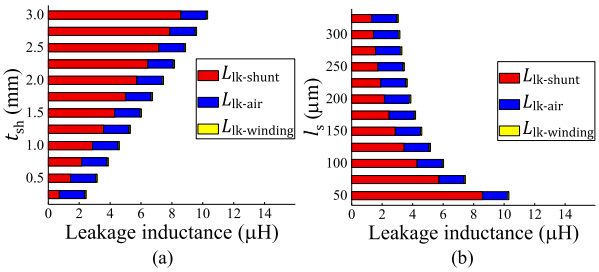

FIGURE 5. Leakage inductance distribution. (a) For different thicknesses of the shunt (t_{sh}), ℓ_s=0.3mm. (b) For different distances from shunts to cores (ℓ_s), t_{sh}=0.5mm. Core: E32/6/20/R-3F4, w_{sh}=2.5mm, N_P=10, N_S=2, n_P=5, n_S=2, k_P=2, k_S=1, x_P= x_S=1.5mm.

model as the inserted-segmental-shunt topology but its inserted shunts are not segmental and can be placed easily.

One might think that inserting one solid low-permeability shunt between two E-cores (presented in [31]) would be easier than overlaying two identical solid shunts on the front and back of the transformer. However, manufacturing a solid shunt from low-permeability materials (e.g., a powder core) is harder and more expensive than manufacturing a solid shunt based on high-permeability materials like ferrite. In addition, low-permeability magnetics have temperature-dependent permeability, leading to unstable leakage inductance.

In the following, the modelling of the proposed structure is discussed for estimation of the leakage and magnetising inductances.

Equation (1) can be used to calculate the leakage inductance, L_{lk}.

$$E = \frac{1}{2}\iiint_V BH\, dV = \frac{1}{2}L_{\rm lk}I_{\rm P}^2 \tag{1}$$

where V is the cuboid that incorporates the magnetic shunt, windows area and windings, I_P is the RMS of primary current, B is the flux density and H is the magnetic field intensity.

From (1), to calculate the leakage inductance, the energy stored in the windows area, and the primary and secondary windings, alongside the inserted shunts need to be calculated. Therefore, the energy stored in each part is calculated separately in the following and then the total leakage inductance can be obtained by summation of energies and from (1).

A. LEAKAGE ENERGY STORED IN WINDOW AREA

The magnetomotive force (MMF) of each layer of the primary winding, $\mathfrak{F}_{\rm P}$, may be obtained from (2), where $k_{\rm P}$ is the number of turns in each layer of the primary winding.

$$\mathfrak{F}_{\rm P} = k_{\rm P}I_{\rm P} \tag{2}$$

If $n_{\rm P}$ and $n_{\rm S}$ are the number of layers of the primary and secondary windings, respectively, then the MMF within the window area, $\mathfrak{F}_{air}$, is equal to $n_{\rm P}\mathfrak{F}_{\rm P}$ and the magnetic field intensity within the air area, H_{air}, may be obtained by (3).

$$H_{air} = \frac{n_{\rm P}\mathfrak{F}_{\rm P}}{b_w} \tag{3}$$

where b_w is the width of the winding area (defined in Fig. 2(b)). From (1), the stored energy of leakage inductance in air area, E_{air}, (defined in Fig. 3) can be calculated as (4).

$$E_{air} = \frac{1}{2}\mu_0 w_c b_w \int_{-x_{\rm S}}^{x_{\rm P}} H_{air}^2 dx \tag{4}$$

where $w_{\rm c}$ is the core depth and $x_{\rm P}$ and $x_{\rm S}$ are the distances from the primary and secondary windings to centre of the transformer, respectively, shown in Fig. 3. By substituting (2) and (3) into (4), E_{air} can be calculated as (5).

$$E_{air} = \mu_0 w_c \frac{n_{\rm P}^2 k_{\rm P}^2 I_{\rm P}^2}{b_w}\,(x_{\rm P} + x_{\rm S}) \tag{5}$$

B. LEAKAGE ENERGY STORED IN PRIMARY AND SECONDARY WINDINGS

According to the MMF distribution presented in Fig. 3(obtained based on method outlined in [26], [29], [30]), the stored

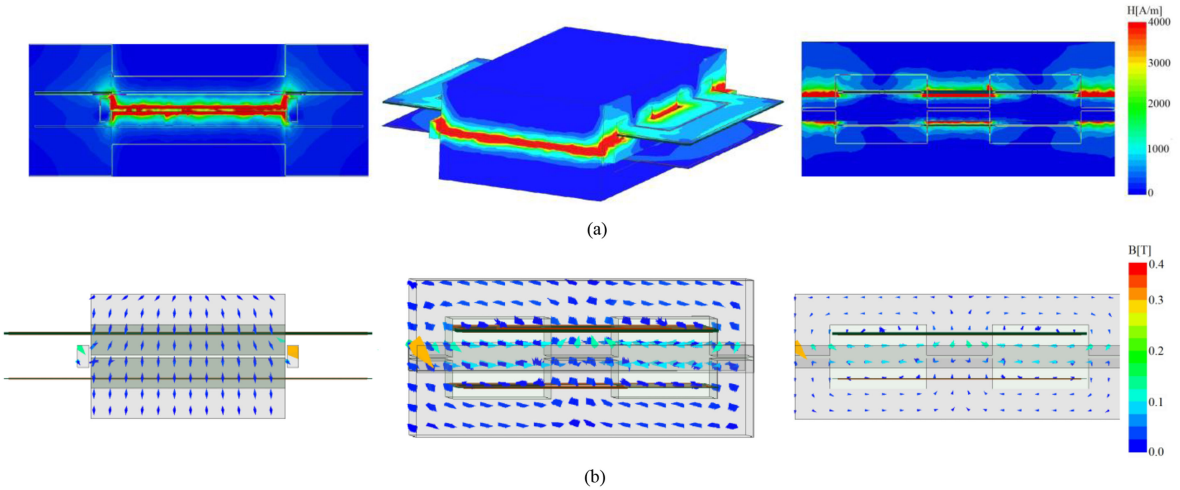

FIGURE 6. FEA simulation results of the proposed topology. (a) Magnetic field intensity. (b) Magnetic flux density vectors. Core: E32/6/20/R-3F4.

TABLE 1 Proposed Structure's Specification

Symbol	Parameter	value
N_P	Primary turns	10
N_S	Secondary turns	2
k_P	Turns per layer in primary	2
k_S	Turns per layer in secondary	1
n_P	Number of primary layers	5
n_S	Number of secondary layers	2
h_P, h_S	Primary and secondary conduction thickness	35 µm
$h_{\Delta P}$, $h_{\Delta S}$	Primary and secondary insulation thickness	30 µm
t_{sh}	Shunt thickness	2.3 mm
w_{sh}	Shunt wideness	1.5 mm
ℓ_g	Transformer air gap	0.28 mm
ℓ_s	Distance between shunt and cores	0.23 mm
x_P, x_S	Distance between primary and secondary windings and centre of cores	1.5 mm 1.5 mm

TABLE 2. Parameters of the Implemented Integrated Transformer

Parameter	Symbol	Modelling	Simulation	Measurement
Magnetising inductance	L_m	28.7 µH	29.15 µH	29.4 µH
Leakage inductance	L_{lk}	10.3 µH	9.3 µH	9.4 µH

energy in PCB layers of primary and secondary windings can be calculated. Ouyang *et al.* [26] proved that energy stored in the primary and secondary windings may be obtained as (6) and (7), respectively.

$$E_P = \frac{1}{6}\mu_0 \frac{w_c}{b_w} k_P^2 \left[h_{\Delta P}(2n_P^3 - 3n_P^2 + n_P) + 2h_P n_P^3\right] I_P^2 \quad (6)$$

$$E_S = \frac{1}{6}\mu_0 \frac{w_c}{b_w} k_S^2 \left[h_{\Delta S}(2n_S^3 - 3n_S^2 + n_S) + 2h_S n_S^3\right] I_S^2 \quad (7)$$

In (6) and (7), h_P and h_S are defined as the thickness of the PCB tracks of the primary and secondary windings, respectively, and $h_{\Delta P}$ and $h_{\Delta S}$ are defined as the thickness of

TABLE 3. The Implemented LLC Converter's Specification

Symbol	Parameter	value
N_P: N_S	Turns ratio	10:2
L_m	Magnetising inductance	29 µH
L_r	Resonant (series) inductance	9 µH
C_r	Resonant capacitance	39 nF
V_{in}	Input voltage	45-55 V
V_{out}	Output voltage	5 V
P_{out}	Output power	25 W
f_s	Switching frequency	200-350 kHz
S	Switches	IRF530N
D	Rectifier diodes	12CTQ045

PCB insulation layers of the primary and secondary windings, respectively.

C. LEAKAGE ENERGY STORED IN MAGNETIC SHUNTS

The energy stored in the shunts can be calculated by the method outlined by Ansari *et al.* [32], [33]. The reluctance model of the proposed topology is presented in Fig. 2(d), where $\mathcal{R}_{g1}$, $\mathcal{R}_{gg}$ and $\mathcal{R}_{g2}$ are air gap reluctances, $\mathcal{R}_{C1}$, $\mathcal{R}_{C2}$ and $\mathcal{R}_{CC}$ are core reluctances and $\mathcal{R}_S$ is shunt reluctance and they can be calculated by (8)–(14). In the reluctance modelling presented in Fig. 2(d), it is assumed both shunts are located at the same distance from the cores (ℓ_s), and therefore they can be considered only one shunt but with double thickness ($2\,t_{sh}$).

$$\mathcal{R}_{C1} = \frac{\ell_{C1}}{\mu_0 \mu_r b_d w_c} \quad (8)$$

$$\mathcal{R}_{C2} = \frac{\ell_{C2}}{\mu_0 \mu_r b_d w_c} \quad (9)$$

$$\mathcal{R}_{CC} = \frac{\ell_{C1}}{\mu_0 \mu_r A_c} \quad (10)$$

$$\mathcal{R}_S = \frac{b_w}{2\mu_0 \mu_s t_{sh} w_{sh}} \quad (11)$$

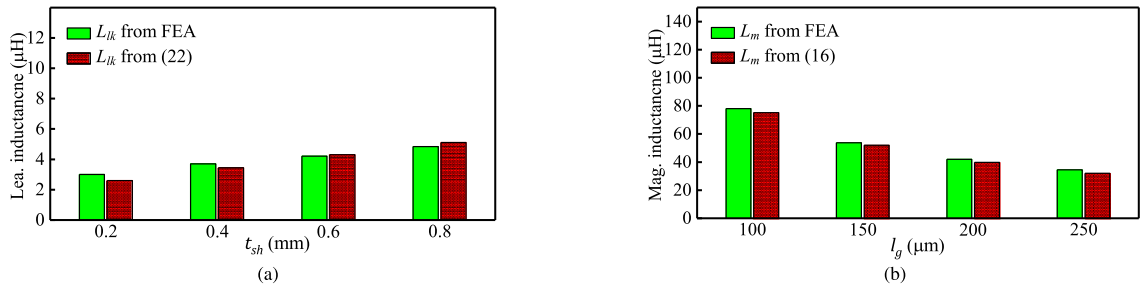

FIGURE 7. Modelling validation by simulation study. (a) Leakage inductance ($\ell_g = 0.05mm$). (b) Magnetising inductance ($t_{sh} = 1mm$). E32/6/20/R-3F4, $\ell_s = 0.2mm$.

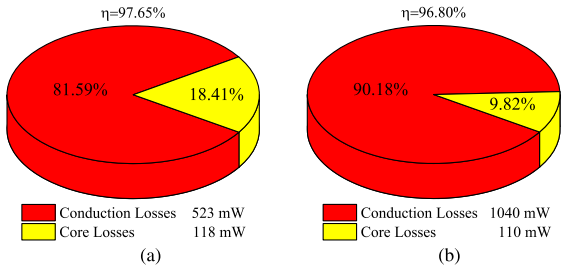

FIGURE 8. Loss distribution. (a) Proposed topology. (b) Inserted-segmental-shunt topology. Core: E32/6/20/R-3F4.

$$\mathcal{R}_{g1} = \frac{\ell_g}{\mu_0 b_d w_c} \tag{12}$$

$$\mathcal{R}_{g2} = \frac{\ell_s}{\mu_0 b_d t_{sh}} \tag{13}$$

$$\mathcal{R}_{gg} = \frac{\ell_g}{\mu_0 A_c} \tag{14}$$

where μ_0 , μ_r and μ_s are the permeability of the air, and the relative permeability of the core and shunt, respectively. A_C is the core effective cross-sectional area and the definition of other quantities can be found in Fig. 2(b). According to the reluctance model presented in Fig. 2(d) and method outlined by Ansari *et al.* [32], [33], leakage inductance due to the inserted magnetic shunts referred to the primary side and magnetising inductance for the proposed topology can be calculated by (15) and (16), respectively.

$$L_{\mathrm{lk-shunt}} = \frac{4N_{\mathrm{P}}^2}{\mathcal{R}_E + 2\left(\mathcal{R}_S + \mathcal{R}_A + \mathcal{R}_B\right)} \tag{15}$$

$$L_{\mathrm{m}} = \frac{2N_{\mathrm{P}}^2(\mathcal{R}_S + \mathcal{R}_A + \mathcal{R}_B)}{\mathcal{R}_E\left(\mathcal{R}_E + 2\left(\mathcal{R}_S + \mathcal{R}_A + \mathcal{R}_B\right)\right)} \tag{16}$$

where N_P is primary turns number ($n_{\mathrm{P}}k_{\mathrm{P}}$) and R_E can be defined as

$$\mathcal{R}_E = \mathcal{R}_{C1} + \mathcal{R}_{C2} + 2\mathcal{R}_{CC} + \mathcal{R}_C + \mathcal{R}_D \tag{17}$$

and $\mathcal{R}_A$, $\mathcal{R}_B$, $\mathcal{R}_C$ and $\mathcal{R}_D$ are defined as follows:-

$$\mathcal{R}_A = \frac{\mathcal{R}_{g2}^2}{\mathcal{R}_{g1} + 2\mathcal{R}_{g2}} \tag{18}$$

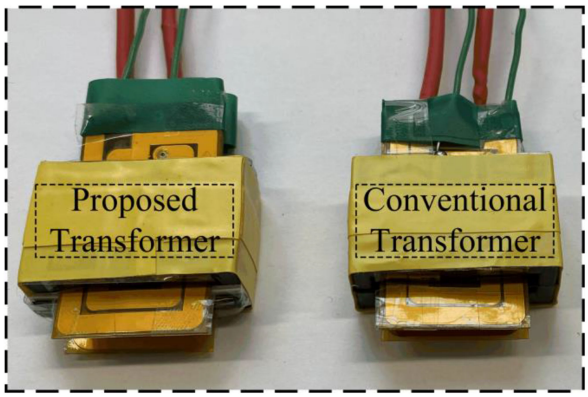

FIGURE 9. Prototypes of the proposed and inserted-segmental-shunt (conventional) topologies. Core: E32/6/20/R-3F4.

$$\mathcal{R}_B = \frac{\mathcal{R}_{g2}^2}{2\mathcal{R}_{gg} + 2\mathcal{R}_{g2}} \tag{19}$$

$$\mathcal{R}_C = \frac{\mathcal{R}_{g1}\mathcal{R}_{g2}}{\mathcal{R}_{g1} + 2\mathcal{R}_{g2}} \tag{20}$$

$$\mathcal{R}_D = \frac{2\mathcal{R}_{gg}\mathcal{R}_{g2}}{2\mathcal{R}_{gg} + 2\mathcal{R}_{g2}} \tag{21}$$

From (1), (5)–(7) and (15), the total leakage inductance of the proposed topology may be obtained by (22).

$$L_{\mathrm{lk}} = 2\mu_0 w_c \frac{N_{\mathrm{P}}^2}{b_w}\left(x_{\mathrm{P}} + x_{\mathrm{S}}\right) + \frac{4N_{\mathrm{P}}^2}{\mathcal{R}_E + 2(\mathcal{R}_S + \mathcal{R}_A + \mathcal{R}_B)} + \frac{1}{3}\mu_0 \frac{w_c}{b_w} k_{\mathrm{P}}^2 n_{\mathrm{P}}^2 \sum_{i=P,S}\left[h_{\Delta i}\left(2n_i - 3 + \frac{1}{n_i}\right) + 2h_i n_i\right] \tag{22}$$

Therefore, (16) and (22) can be used to design an integrated transformer according to the required magnetising and leakage inductances.

To demonstrate the fidelity of control achievable with the proposed topology, the calculated leakage and magnetising inductances for the proposed topology for different thickness of the shunt, t_{sh}, and air-gap lengths, ℓ_{g} and ℓ_{s}, are presented in Figs. 4(a) and (b), respectively. It can be seen that the magnetising inductance is only influenced by air-gap length

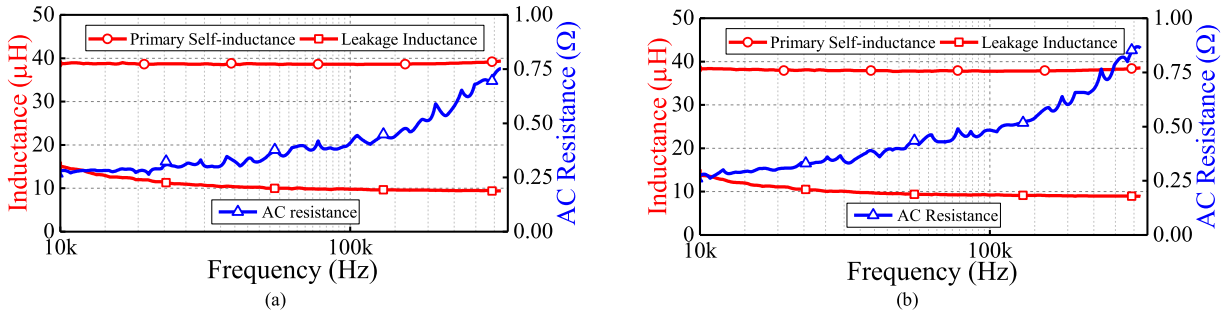

FIGURE 10. **AC resistance, primary self-inductance and leakage inductance versus frequency. (a) Proposed topology. (b) Inserted-segmental-shunt topology.**

between cores (ℓ_g) and is not significantly affected by changing the thickness of the shunt and ℓ_s. On the other hand, the leakage inductance is mainly affected by the distance between shunts and cores (ℓ_s) and also the thickness of the shunt (t_{sh}). Hence, in the proposed structure, the leakage and magnetising inductances are decoupled from each other and can be regulated separately, leading the design process to higher flexibility.

The leakage inductance distribution (between shunt, air and winding) of the proposed integrated transformer for different thicknesses of the shunt (t_{sh}) and distances from shunts to cores (ℓ_s) are shown in Figs. 5(a) and (b), respectively. As shown, the leakage inductance (L_{lk}) is mainly affected by shunt dimensions and ℓ_s. The leakage inductance, caused by the window area (L_{lk-air}) and windings ($L_{lk-winding}$), is only affected by the geometries of the core and PCB windings.

The characteristics of the proposed integrated transformer are now fully investigated and it is shown that the transformer can be designed for most reasonable specifications of leakage and magnetising inductances. It does not need any low-permeability materials or segmental shunts. Therefore, the proposed transformer is a great candidate for use in an LLC resonant converter where it can integrate the magnetic components into only a single transformer. In the following, the operation of the proposed transformer when it is designed to be used in a typical LLC resonant converter is investigated and its modelling is verified by simulation and experimental results.

III. SIMULATION RESULTS

To verify the theoretical analysis presented in Section II, FEA simulation of the proposed integrated transformer is provided. Therefore, an integrated transformer is designed and its specification is presented in Table 1. The leakage and magnetising inductances and the turns ratio of the designed transformer are selected according to the specification of an exemplar isolated LLC resonant converter presented in Table 3. The transformer core (E32/6/20/R-3F4) is selected based on the design guidlines outlined by core manufacturer in its catalogue [35], which provides charts indicating the appropriate core according to the stored energy and operating frequency. The thickness of the shunt and air-gap lengths (ℓ_g and ℓ_s) are estimated

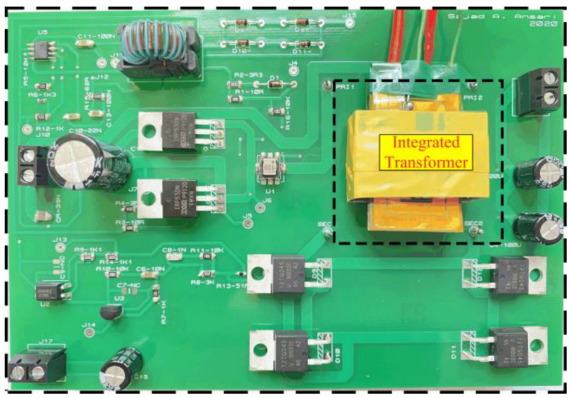

FIGURE 11. **Prototype of the designed LLC converter. .**

in order to provide the required leakage and magnetising inductances using (16) and (22) and considering the dimensions of the selected core. In addition, the windings are designed considering the dimensions, skin effect, their root-mean-square (RMS) currents and the difficulty of manufacturing.

The magnetic field intensity and flux density vectors for the proposed integrated transformer, while it is used in an LLC converter with specification presented in Table III, are shown in Figs. 6(a) and (b), respectively. According to Fig. 6, the magnetic field intensity and flux density vectors are dominant in the shunts and their air gaps (ℓ_s) rather than window area and PCB windings. The leakage flux and, therefore, inductance is mainly caused by the shunts. In addition, since the magnetic field intensity is highest in the core air gap (ℓ_g), the magnetising inductance is mainly affected by ℓ_g. The leakage and magnetising inductances versus thickness of the shunt (t_{sh}) and transformer air gap (ℓ_g) obtained from (16) and (22) and measured by FEA simulation are presented for the proposed topology in Figs. 7(a) and (b), respectively. Fig. 7 shows a good agreement between the theoretical and simulation results, verifying the analysis of the proposed structure.

The loss distribution and efficiency of the proposed topology and that of the segmental-shunt topology ,while they are used in the LLC converter at nominial operation, were calculated using FEA and are presented in Figs. 8(a) and (b), respectively. As shown, the proposed topology benefits

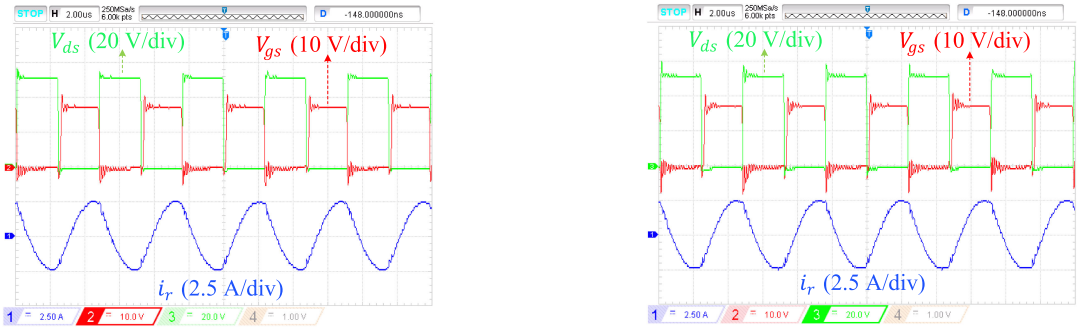

FIGURE 12. Experimental waveforms of the designed LLC converter. (a) Using proposed topology. (b) Using the inserted-segmental-shunt topology. V_{ds} is drain to source voltage, V_{gs} is gate to source voltage and i_r is the resonant current (defined in Fig. 1).

from lower conduction losses and therefore provides higher efficiency.

IV. EXPERIMENTAL VERIFICATION

To verify theoretical analysis and simulation results, an integrated transformer based on the proposed structure with specification presented in Table I is built and its prototype is shown in Fig. 9. In addition, a recent proposed integrated transformer with inserted-segmental-shunt presented in [32], [33] is built with the same specification and is compared with the proposed topology, shown in Fig. 9.

The measured leakage and magnetising inductances of the proposed topology at 200 kHz measured by an Omicron Bode 100 analyser are shown in Table 2. The measured values are close to the values obtained by modelling and simulation results. In addition, the AC resistance, primary self-inductance and leakage inductance versus frequency for the proposed topology and the segmental shunt topology are shown in Figs. 10(a) and (b), respectively. The measurement was carried out by the precision impedance analyser Omicron Bode 100 while the windings and shunt were located inside the planar cores. As shown in Fig. 10, both transformers have similar magnetising and leakage inductances. However, the AC resistance of the topology with inserted segmental shunt is higher than the proposed topology because of its high fringing losses (as mentioned in [32], [33]). As seen in Fig. 2, in the proposed topology, the air-gaps of the shunt (labelled ℓ_s) are further from the windings, reducing their coupling with the fringing field and hence reducing losses. In the segmental topology, the air gaps are between the lower and upper parts of the winding and therefore have greater coupling and therefore greater losses.

To verify the performance of the proposed integrated transformer in practice, an LLC resonant converter is implemented with the specification presented in Table 3 calculated according to the design procedure outlined in [36], as shown in Fig. 11. In this design, the series and parallel inductances are integrated into the transformer. The waveforms of the converter operating at 210 kHz using (a) the proposed topology and (b) the topology with inserted-segmental-shunt are shown in Fig. 12. It can be seen that the switches are turned on at zero voltage (ZVS) because the switch gate turns on after its drain-source voltage drops to zero.

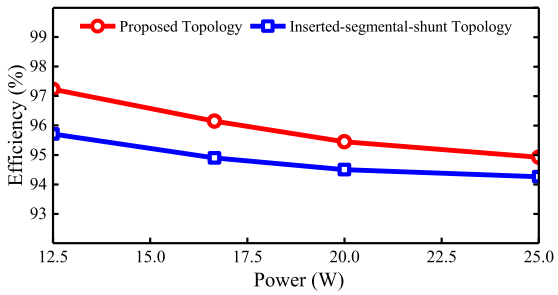

FIGURE 13. Efficiency of the designed LLC converter without the rectifier stage using the proposed inserted-solid-shunt and conventional inserted-segmental-shunt integrated transformers.

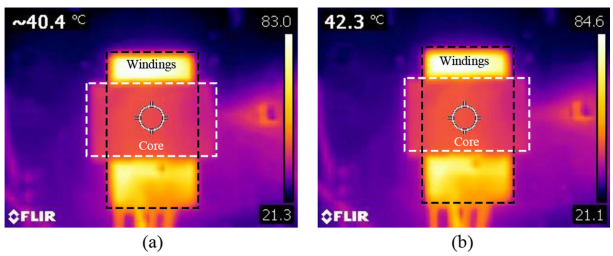

FIGURE 14. Thermal image of the transformer. (a) Proposed topology. (b) Inserted-segmental-shunt topology.

The efficiency of the implemented LLC converter using the proposed integrated transformer and inserted-segmental-shunt integrated transformer are shown in Fig. 13 for different output powers. It can be seen that, since the topology with inserted-segmental-shunt suffers from higher AC resistance, it has a lower efficiency compared to the proposed topology. The efficiency of the converter is evaluated after removing the rectifier stage from the circuit since the losses from an asynchronous rectifier are higher than losses in the magnetics. Rectifier design is not the focus of this work and thus the rectifier is not optimized.

Thermal images of the proposed topology and inserted-segmental-shunt transformer at nominal operating conditions are shown in Figs. 14(a) and (b), respectively. It can be seen

that the proposed transformer has a lower temperature (about 2 °C) compared to the inserted-segmental-shunt transformer since it benefits from lower losses. In addition, the windings have a higher temperature compared to the cores since they have higher losses, which confirms the loss distribution presented in Fig. 8.

It should be noted that the application of the proposed integrated transformer can be extended to other converters such as the phase-shifted full-bridge converters and dual-active-bridge converters and is not only restricted to the LLC resonant converter.

To sum up, not only does the proposed shunt-inserted integrated transformer address the main issues of the segmental shunt topology, but it also provides a higher efficiency without fundamentally redesigning the planar transformer or its associated converter.

V. CONCLUSION

A new topology for the shunt-inserted integrated planar transformers is proposed. The inserted shunts are solid in the proposed topology, leading to easier manufacturing compared to segmental shunt topology. In addition, the shunts are based on high-permeability materials like ferrite, which is widely available in the market with different sizes and lower price. Therefore, the proposed structure benefits from both advantages of the high-permeability segmental shunt and low-permeability one-segment shunt topologies. The analysis and modelling of the proposed structure are presented. The leakage and magnetising inductances are decoupled from each other in the proposed structure and can be regulated separately, leading to a flexible design process. FEA simulation and experimental implementation are provided to verify the theoretical analysis. In addition, according to the presented results, the proposed topology can provide a higher efficiency compared to the inserted-segmental-shunt topology. An LLC resonant converter is also implemented to examine the performance of the proposed integrated transformer in practice. The prototype shows that the proposed topology can integrate all the three magnetic components of the LLC converter into a single planar transformer.

REFERENCES

[1] K. Nathan, S. Ghosh, Y. Siwakoti, and T. Long, "A new DC–DC converter for photovoltaic systems: Coupled-inductors combined Cuk-SEPIC converter," *IEEE Trans. Energy Convers.*, vol. 34, no. 1, pp. 191–201, Mar. 2019.

[2] S. A. Ansari and J. S. Moghani, "A novel high voltage gain noncoupled inductor SEPIC converter," *IEEE Trans. Ind. Electron.*, vol. 66, no. 9, pp. 7099–7108, Sep. 2019.

[3] A. Mirzaee, S. Arab Ansari, and J. Shokrollahi Moghani, "Single switch quadratic boost converter with continuous input current for high voltage applications," *Int. J. Circuit Theory Appl.*, vol. 48, no. 4, pp. 587–602, 2020.

[4] A. Mizani, S. A. Ansari, A. Shoulaie, J. N. Davidson, and M. P. Foster, "Single-active switch high-voltage gain DC–DC converter using a noncoupled inductor," *IET Power Electron.*, vol. 14, pp. 492–502, 2021.

[5] S. A. Ansari, A. Mizani, J. S. Moghani, and A. Shoulaie, "A new high step-up gain SEPIC converter for renewable energy applications," in *Proc. 10th Int. Power Electron., Drive Syst. Technol. Conf.*, 2019, pp. 539–544.

[6] S. A. Ansari and J. S. Moghani, "Soft switching flyback inverter for photovoltaic AC module applications," *IET Renewable Power Gener.*, vol. 13, no. 13, pp. 2347–2355, 2019.

[7] S. A. Ansari, J. N. Davidson, and M. P. Foster, "Evaluation of silicon MOSFETs and GaN HEMTs in soft-switched and hard-switched DC-DC boost converters for domestic PV applications," *IET Power Electron.*, vol. 14, pp. 1032–1043, 2021.

[8] S. Arab Ansari, J. S. Moghani, and M. Mohammadi, "Analysis and implementation of a new zero current switching flyback inverter," *Int. J. Circuit Theory Appl.*, vol. 47, no. 1, pp. 103–132, 2019.

[9] H.-P. Park, M. Kim, and J. Jung, "Bidirectional current-fed CLLC resonant converter employing asymmetric PWM," *IEEE Trans. Energy Convers.*, vol. 36, no. 4, pp. 3167–3177, Dec. 2021.

[10] Y. Wei, Q. Luo, and A. Mantooth, "Overview of modulation strategies for LLC resonant converter," *IEEE Trans. Power Electron.*, vol. 35, no. 10, pp. 10423–10443, Oct. 2020.

[11] Z. Fang, Z. Huang, H. Jing, and F. Liu, "Hybrid mode-hopping modulation for LLC resonant converter achieving high efficiency and linear behaviour," *IET Power Electron.*, vol. 13, no. 6, pp. 1153–1162, 2020.

[12] C. W. Tsang, M. P. Foster, D. A. Stone, and D. T. Gladwin, "Analysis and design of LLC resonant converters with capacitor–diode clamp current limiting," *IEEE Trans. Power Electron.*, vol. 30, no. 3, pp. 1345–1355, Mar. 2015.

[13] Y. Zhang, D. Xu, K. Mino, and K. Sasagawa, "1MHz-1kW LLC resonant converter with integrated magnetics," in *Proc. Twenty-Second Annu. IEEE Appl. Power Electron. Conf. Expo.*, 2007, pp. 955–961.

[14] J. Wang *et al.*, "Design of integrated magnetic transformer for high frequency LLC converter," in *Proc. 4th Int. Conf. HVDC*, 2020, pp. 986–991.

[15] S.-Y. Yu, C. Hsiao, and J. Weng, "A high frequency CLLLC Bi-directional series resonant converter DAB using an integrated PCB winding transformer," in *Proc. IEEE Appl. Power Electron. Conf. Expo.*, 2020, pp. 1074–1080.

[16] M. H. Ahmed, A. Nabih, F. C. Lee, and Q. Li, "Low-loss integrated inductor and transformer structure and application in regulated LLC converter for 48-V bus converter," *IEEE J. Emerg. Sel. Topics Power Electron.*, vol. 8, no. 1, pp. 589–600, Mar. 2020.

[17] S. Stegen and J. Lu, "Structure comparison of high-frequency planar power integrated magnetic circuits," *IEEE Trans. Magn.*, vol. 47, no. 10, pp. 4425–4428, Oct. 2011.

[18] A. Kats, G. Ivensky, and S. Ben-Yaakov, "Application of integrated magnetics in resonant converters," in *Proc. Appl. Power Electron. Conf.*, 1997, vol. 2, pp. 925–930.

[19] Y. Liu, H. G. Wu, J. Zou, Y. Tai, and Z. Ge, "CLL resonant converter with secondary side resonant inductor and integrated magnetics," *IEEE Trans. Power Electron.*, vol. 36, no. 10, pp. 11316–11325, Oct. 2021.

[20] R. Muhammad, S. Kim, C. Suk, S. Choi, B. Yu, and S. Park, "Integrated planar transformer design of 3-kW auxiliary power module for electric vehicles," in *Proc. IEEE Energy Convers. Congr. Expo.*, 2020, pp. 1239–1243.

[21] J. Biela and J. W. Kolar, "Analytic model inclusive transformer for resonant converters based on extended fundamental frequency analysis for resonant converter-design and optimization," *IEEJ Trans. Ind. Appl.*, vol. 126, no. 5, pp. 568–577, 2006.

[22] B. Li, Q. Li, and F. C. Lee, "High-frequency PCB winding transformer with integrated inductors for a bi-directional resonant converter," *IEEE Trans. Power Electron.*, vol. 34, no. 7, pp. 6123–6135, Jul. 2019.

[23] M. D'Antonio, S. Chakraborty, and A. Khaligh, "Planar transformer with asymmetric integrated leakage inductance using horizontal air gap," *IEEE Trans. Power Electron.*, vol. 36, no. 12, pp. 14014–14028, Dec. 2021.

[24] S. De Simone, C. Adragna, and C. Spini, "Design guideline for magnetic integration in LLC resonant converters," in *Proc. Int. Symp. Power Electron., Elect. Drives, Automat. Motion*, 2008, pp. 950–957.

[25] Z. Ouyang, W. G. Hurley, and M. A. Andersen, "Improved analysis and modeling of leakage inductance for planar transformers," *IEEE J. Emerg. Sel. Topics Power Electron.*, vol. 7, no. 4, pp. 2225–2231, Dec. 2019.

[26] Z. Ouyang, J. Zhang, and W. G. Hurley, "Calculation of leakage inductance for high-frequency transformers," *IEEE Trans. Power Electron.*, vol. 30, no. 10, pp. 5769–5775, 2014.

[27] W. Liu and J. Van Wyk, "Design of integrated LLCT module for LLC resonant converter," in *Proc. Twentieth Annu. IEEE Appl. Power Electron. Conf. Expo.*, 2005, vol. 1, pp. 362–368.

[28] B. Yang, R. Chen, and F. C. Lee, "Integrated magnetic for LLC resonant converter," in *Proc. Seventeenth Annu. IEEE Appl. Power Electron. Conf. Expo. (Cat. No. 02CH37335)*, 2002, vol. 1, pp. 346–351.
[29] J. Zhang, Z. Ouyang, M. C. Duffy, M. A. Andersen, and W. G. Hurley, "Leakage inductance calculation for planar transformers with a magnetic shunt," *IEEE Trans. Ind. Appl.*, vol. 50, no. 6, pp. 4107–4112, Nov./Dec. 2014.
[30] M. Li, Z. Ouyang, B. Zhao, and M. A. Andersen, "Analysis and modeling of integrated magnetics for LLC resonant converters," in *Proc. 43rd Annu. Conf. IEEE Ind. Electron. Soc.*, 2017, pp. 834–839.
[31] M. Li, Z. Ouyang, and M. A. Andersen, "High-frequency LLC resonant converter with magnetic shunt integrated planar transformer," *IEEE Trans. Power Electron.*, vol. 34, no. 3, pp. 2405–2415, Mar. 2019.
[32] S. A. Ansari, J. N. Davidson, and M. P. Foster, "Analysis, design and modelling of two fully-integrated transformers with segmental magnetic shunt for LLC resonant converters," in *Proc. 46th Annu. Conf. IEEE Ind. Electron. Soc.*, 2020, pp. 1273–1278.
[33] S. Arab Ansari, J. Davidson, and M. Foster, "Fully-integrated planar transformer with a segmental shunt for LLC resonant converters," *IEEE Trans. Ind. Electron., early access*, Oct. 2021, doi: 10.1109/TIE.2021.3116574.
[34] S. A. Ansari, J. N. Davidson, M. P. Foster, and D. A. Stone, "Design and analysis of a Fully-integrated planar transformer for LCLC resonant converters," in *Proc. 23rd Eur. Conf. Power Electron. Appl.*, 2021, pp. P. 1–P. 8.
[35] Magnetics Ferrite Catalog, Magnetics, 2013. [Online]. Available: www.mag-inc.com
[36] S. De Simone, "LLC resonant half-bridge converter design guideline," *STMicroelectronics*, Application Note AN2450, 2014, p. 35.

SAJAD A. ANSARI was born in Shahrood, Iran, in 1994. He received the B.S. degree in electrical engineering from the Shahrood University of Technology, Shahrood, Iran, in 2016, and the M.S. degree in electrical engineering from the Amirkabir University of Technology, Tehran, Iran, in 2019. He is currently working toward the Ph.D. degree with the Department of Electronic and Electrical Engineering, The University of Sheffield, Sheffield, U.K. His research interests include renewable energy and design and control of power electronic converters.

JONATHAN N. DAVIDSON received the M.Eng. degree in electronic engineering and the Ph.D. degree in thermal modeling and management from The University of Sheffield, Sheffield, U.K., in 2010 and 2015, respectively. In 2015, he became a Lecturer of electrical engineering with The University of Sheffield. His research interests include thermal modeling and management of power electronics, and the design and analysis of piezoelectric transformer-based power converters, high-voltage power supplies for plasma chemistry, and wastewater sensing systems.

MARTIN P. FOSTER received the B.Eng. degree in electronic and electrical engineering, the M.Sc. (Eng.) degree in control systems, and the Ph.D. degree for his thesis "Analysis and Design of High-order Resonant Power Converters" from The University of Sheffield, Sheffield, U.K., in 1998, 2000, and 2003, respectively. Since 2003, he has been a Member of the academic staff with the Department of Electronic and Electrical Engineering, The University of Sheffield, where he is involved in power electronic systems. His current research interests include the modeling and control of switching power converters, resonant power supplies, multilevel converters, battery management, piezoelectric transformers, power electronic packaging, and autonomous aerospace vehicles.